Droplet formation by pressure-driven flow in T and X-junction microfluidic devices

Aaron Delahanty
BSc Mechanical Engineering
School of Engineering
College of Science and Engineering
University of Glasgow

Submitted in fulfillment of the requirements for the Degree of

Master of Science

2016

Abstract

Microfluidic devices generally require precise control of fluid flowrates in order to accurately and reliably perform their various functions. In the case of droplet-makers fluid flow may be manipulated to dictate the size, frequency and distribution of droplets. Multiple approaches may be taken in order to control fluid flow in such devices. Here a pressure-driven flow controller (PDFC) is developed and characterized for use as a flow provider for droplet-makers and as a tool for further microfluidics-based research.

Previously, droplet-makers that utilize volumetric flow control have been used to define the relationship between continuous and discontinuous phase flowrates and the resulting droplet parameters and flow regimes. Here pressure-driven droplet-makers are characterized and compared to the existing systems. Furthermore, an investigation into the ability to control droplet formation in real-time is conducted by quantifying the time-to-stability of the electronic flow controller and droplet-maker system.

The work conducted and presented here can be divided clearly into three sections (i) design, fabrication, development of the PDFC (ii) characterization of the PDFC system and (iii) investigation into the behavior of droplet-maker devices as driven by pneumatic pressure.

The PDFC system consists of a micro controller, sensing pressure transducers, regulating pressure transducers, as well as various pneumatic and electronic components used to integrate the system into University of Glasgow's Franke Lab's existing microfluidic test set-up. The system was characterized to show pressure control ranging from 0 to 1000mbar with 4 discreetly controlled channels capable of precision of XX with a time response of XX. When applied as the flow controller for droplet-makers it was found that droplet formation as defined by length:width behaved similarly to previously volumetric flow rate systems.

A major limitation of pressure-driven flow systems is that the flow rate within microfluidic devices varies as a function of device geometry. Herein significant discussion is presented as to methods of theoretical and experimental approximations of the volumetric flowrates resulting from pressure-driven flow.

Contents

List of Figures

Chapter 1

System Application - Droplet Microluidics

1.1 Aims

The application of the PDFC to droplet microfluidics serves two purposes. First, it verifies that the system is functioning as intended for use as a research tool. Second, it allows the characterization of droplet formation by a pressure driven flow in conjunction with X and T-junction geometry, an area currently underdeveloped [ref]. These aims can be fufilled by the following two objectives:

1. Determine how applied pressure determine droplet formation regime
2. Relate applied pressure to droplet scaling law [14]

1.2 Methods

1.2.1 Device Generation

1.2.2 Experimental Procedure

Droplet formation was captured on a high speed camera at 2.5k to 20k frames per second. The applied control pressure was held constant for the continuous phase at a nominal value of 400mbar while varying the discontinuous phase control pressure. Discontinuous phase control pressure was varied at intervals of ≈10mbar above and below the nominal 400mbar until droplet formation ceased due to the onset of backflow or jetting, for low or high pressures, respectively. The captured images were then analyzed using a custom imageJ script to determine droplet length, L, and position, X, along an arbitrarily defined axis parallel to the geometry's outlet channel.

1.3 Results

For both X-junction and T-junction channel geometries L is plotted as a function of the applied control pressure ratios, $\frac{P_{H_2O}}{P_Oil}$, shown in Figure 1.1. Outer Ca values are calculated at the transition between flow regimes given an interfacial tension of $\gamma = 2.87 \times 10^{-3} \frac{N}{m}$, continuous phase viscosity of $\mu = 1.24 \times 10^{-3} Pa \cdot s$, and mean velocities, u, as determined by droplet x-position.

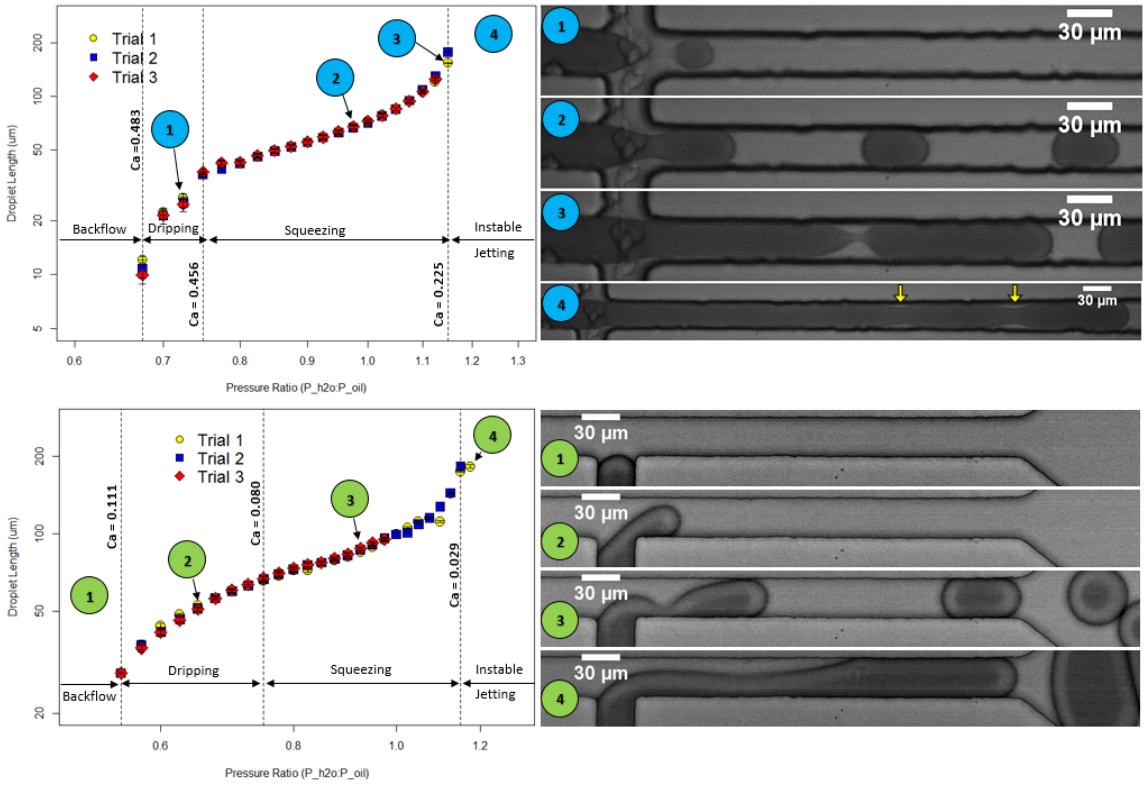

Figure 1.1: Log-Log plots of droplet length as a function of the applied control pressure ratio for X-junction(top) and T-junction(bottom) geometry. Select images are shown for each geometry showing the case of quasi-equilibrium (bottom-1), droplet formation within the dripping regime (top-1, bottom-2), droplet formation within the squeezing regime (top-2, bottom-3), migration of the 'pinch-point' along the longitudinal axis (top-3, bottom-4), and onset of jetting (top-4).

1.4 Discussion

Previous work has been done to establish specific flow regimes in which droplets are formed in T-junction geometry by both modeling and experimental investigations [1],[6],[7]. The findings suggest that two stable droplet formation regimes exist (i) *dripping* - in which the viscous forces associated with the continuous phase flow are significantly large to cause shearing of the immiscible thread and the production of a droplet prior to blocking the outlet channel and (ii) *squeezing* - in which the immiscible thread blocks the majority of the outlet channel prior to collapse and droplets are formed by a squeezing effect due to the pressure build up caused by the blocked channel. Investigation into the factors, often expressed as the Capillary Number, Ca, dimensionless group, that dictate regime change is generally conducted using volumetrically controlled flow systems, most often syringe pumps. It has been shown that pressure controlled flow systems produce droplets in a behavior unique from volumetrically controlled systems, despite the accepted generalization that pressure and flow are linearly related in single phase systems [12], shown without permission in Figure 1.2. Here for the first time, experimental data is shown presenting droplet formation as defined by L/w as a function of control-pressure ratio with a specific emphasis on flow regime and corresponding Ca values.

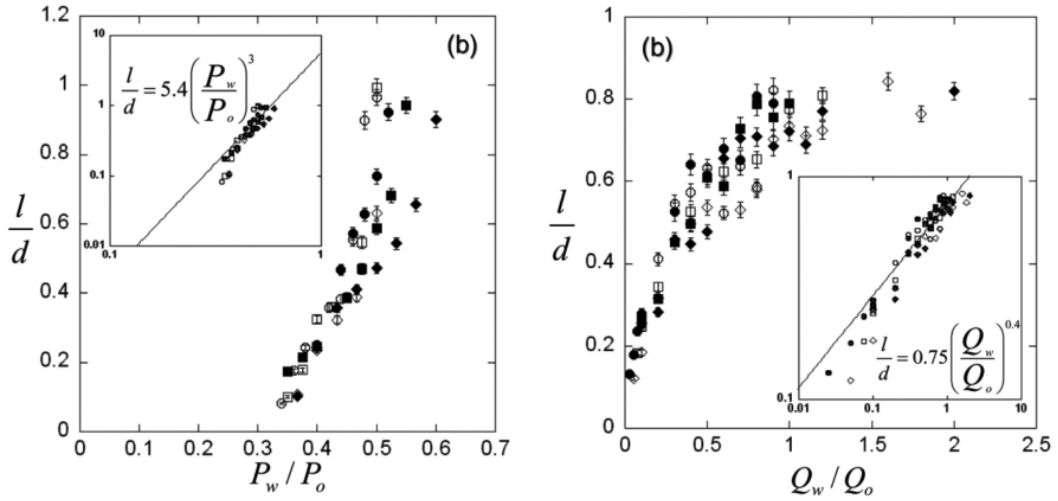

Figure 9. (a) Distance between the center of mass of two consecutive drops *versus* inlet pressure ratio. (b) Dimensionless drop length *l*/*a versus* flow-rate ratio. The inset shows the same data plotted in log-log coordinates, where the solid line has slope 3, which appears the fit the data over two decades of the flow rate ratio P_w/P_o.

Figure 7. (a) Distance *d* between the center of mass of two consecutive drops *versus* the flow-rate ratio. (b) Dimensionless drop length *l*/*a versus* flow-rate ratio. The inset shows the same data plotted in log-log coordinates, where the solid line has slope 0.4, which appears to fit the data over two decades of the flow rate ratio Q_w/Q_o.

Figure 1.2: Used without permission, taken directly from [12]

In this experiment both interfacial tension and viscosities are assumed constant and therefore the only variable affecting the *Ca* value is the mean velocity which in this case is approximated by direct measurement of the droplet velocity. It is expected that there is some numerical difference between the velocity of the droplets and the velocity of the continuous phase but we assume this difference is sufficiently small as to be neglected[12] [could use additional REF]. In the system developed here, the only inputs used to manipulate flow behavior are the two applied pressures. Therefore, in order to characterize the system's flow regimes it is logical to determine the relationship between applied pressures and the resulting droplet velocity. Here, velocity is plotted as a function of the applied pressure ratio for both T and X-junctions as shown in Figure 1.3. Ward determined the relationship for their system as shown in Figure 1.4 on the next page. (XX we need to do the same)

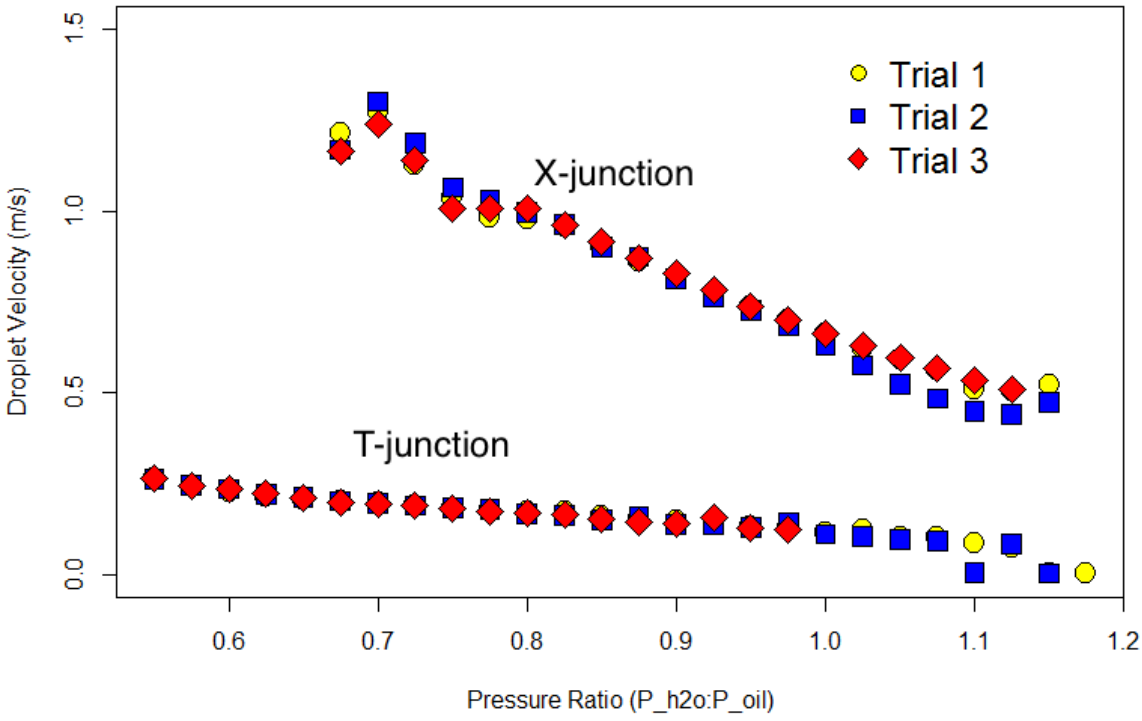

Figure 1.3: Droplet velocity for both T and X-junctions

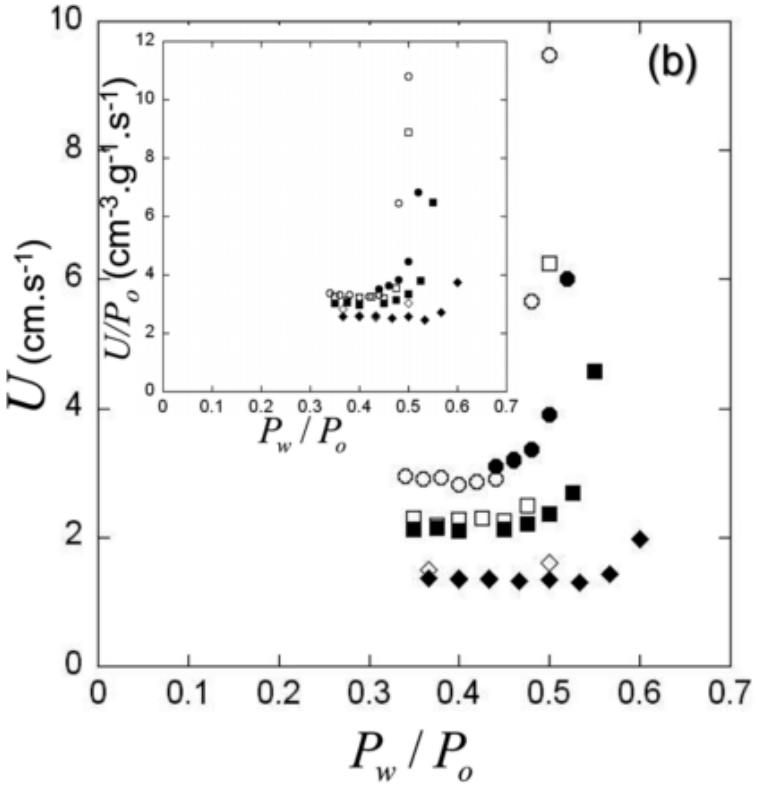

Figure 3. Measured velocity *U versus* (a) flow-rate where o, ● Q_o = 2000 μL/h, □, ■ Q_o = 1000 μL/h and (◇, ◆ Q_o = 500 μL/h and (b) inlet pressure ratio where o, ● P_o = 12.5 Psi, □, ■ P_o = 10 Psi and ◇, ◆ P_o = 7.5 Psi. The open and closed symbols are for experiments where the dispersed phase fluid flow parameter is either increased or decreased respectively.

Figure 1.4: Used without permission, taken directly from [12]

Two important observations:

1. The system used here is operating at velocities approximately a magnitude greater than Ward's system (1m/s vs 1cm/s)

2. The relationship between velocity and applied pressure ratios are different. Our system shows a relatively linear and slightly downward trending velocity while in Ward's case velocity is relatively flat then at some critical pressure increases exponentially.

From the droplet velocity Ca and Re values can be determined. Again, Ca is considerably higher than reported by others [6], [12] . A plot of droplet length versus Ca value is shown in Figure 1.5.

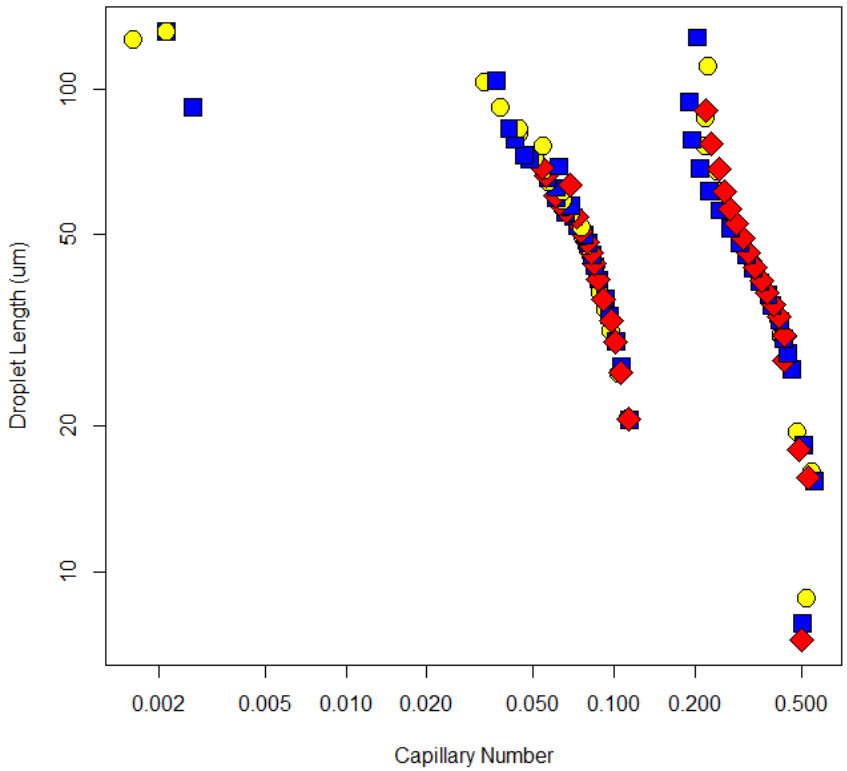

Figure 1.5: Log-Log plot Capillary Number as a function of Applied Control Pressure Ratio

Using the determined velocities Ca and Re numbers are calculated as shown in Figure **??** on page ??

	A	B	C	D	E	I	J	K	L	M
1						Velocity				
2	Note	Voil	Poil(bar)	Vh2o	Ph2o(bar)	T (m/s)	MEAN(m/s)	**Ca**	Flowrate (L/s)	**Re**
3	T-drip/noflow	2	0.4	1.1	0.22	0.266606867				
4		2	0.4	1.1	0.22	0.259131908				
5		2	0.4	1.1	0.22	0.246673643	0.257470806	**0.111242**	2.31724E-07	**10.05382**
6	Tdrip-squeeze	2	0.4	1.5	0.3	0.188119799				
7		2	0.4	1.5	0.3	0.184382319				
8		2	0.4	1.5	0.3	0.185628146	0.186043421	**0.080381**	1.67439E-07	**7.264696**
9	Tsqueeze-jet	2	0.4	2.3	0.46	0.066028804				
10		2	0.4	2.3	0.46	0.069766283				
11		2	0.4	2.3	0.46	0.068520456	0.068105181	**0.029425**	6.12947E-08	**2.659397**
12	X-drip/noflow	2	0.4	1.35	0.27	1.016594409				
13		2	0.4	1.35	0.27	1.106293915				
14		2	0.4	1.35	0.27	1.235859869	1.119582731	**0.483722**	1.00762E-06	**43.7179**
15	Xdrip-squeeze	2	0.4	1.5	0.3	1.061444162				
16		2	0.4	1.5	0.3	1.05147755				
17		2	0.4	1.5	0.3	1.05147755	1.054799754	**0.455732**	9.4932E-07	**41.18823**
18	Xsqueeze-jet	2	0.4	2.3	0.46	0.518263816				
19		2	0.4	2.3	0.46	0.518263816				
20		2	0.4	2.3	0.46	0.528230428	0.52158602	**0.225354**	4.69427E-07	**20.36709**
21										
22	**Constants**	Value	Units	Ref						
23	m/pixel	4.98E-07								
24	Oil Visc	0.00124	Pa-s@25d(	DataSheet						
25	Oil Density	1614	Ns^2/m^4							
26	Interfacial Tensio	0.00287	N/m	unknown						
27	Channel Area	9E-10	m^2							
28	Channel width	0.00003	m^2							

Figure 1.6: Re Ca Calculations

In order to qualitatively characterize the formation of droplets across the entire range of functional pressure ratios, the following section will describe the system behavior at the states of no-flow, dripping, squeezing, and jetting. Due to the strong similarities in droplet-formation behavior between the X-junction and T-junction geometry they will be discussed in general terms with specific metrics given for each case.

No-Flow As the system is moved towards the lowest operational pressure ratios, the aqueous phase comes to a a quasi equilibrium no-flow state. As previously reported by Ward et al citeWard2005 . If the pressure ratio is decreased any further(either by increasing P_{Oil} or decreasing P_{H_2O}) back-flow will occur, in which the continuous phase begins displacing the aqueous phase upstream towards the reservoir. This quasi equilibrium state may be described as a balance of forces between the pressure of the two phases and the Laplace pressure differential across the liquid-liquid interface, described as shown in Equation 1.1.

$$P_{H_2O*} + P_{Laplace} = P_{Oil*} \tag{1.1}$$

Where Laplace pressure can be roughly approximated given γ is the interfacial tension between the two phases, r is the radius of curvature of the interface as:

$$P_{Laplace} = \frac{2\gamma}{r} \tag{1.2}$$

It should be noted that here P_{H_2O*} and P_{Oil*} represent the pressures of the two phases local to the X or T junction and that there is some unknown pressure drop between the applied control pressures at the inlet reservoirs and these local pressures. This pressure drop is dependent on device geometry as well as solution viscosity and can be determined by Hagan-Poiseuille approximations (XX - needs to be done).

Dripping As the control pressure applied to the discontinuous phase is increased beyond the *no-flow* state the immiscible thread begins to extend into the device's channel junction.

Squeezing The pinch point moving further downstream is a manifestation of the increases in tangental viscous forces relative to inertial forces (Ca). The Ca value increases due to the increase in velocity as the interfacial tension and viscosity are both constant. The viscous forces acting tangentially to the discontinuous phase

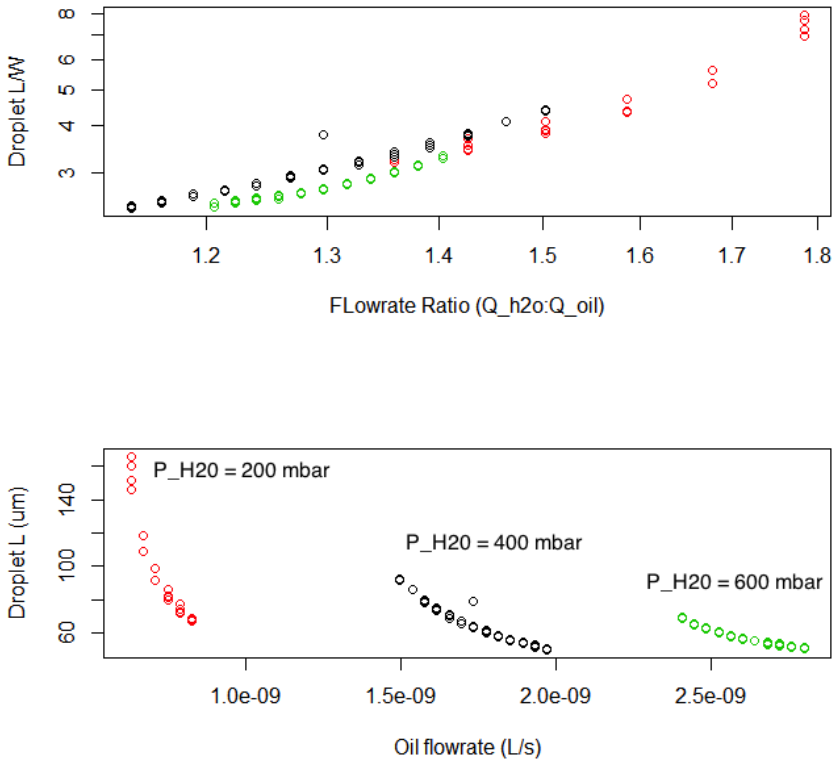

Figure 1.7: Droplet length at varying flowrates

boundary elongates the immiscible thread before the combined effect of increased plugging pressure and inertial forces finally dominate leading to droplet formation.

Bibliography

[1] Adam R. Abate, Pascaline Mary, Volkert van Steijn, and David A. Weitz. Experimental validation of plugging during drop formation in a T-junction. *Lab on a Chip*, 12(8):1516, 2012.

[2] Henrik Bruus. *Theoretical Microfluidics*. Oxford ; New York : Oxford University Press, 2008., 2008.

[3] Lorenzo Capretto, Wei Cheng, Martyn Hill, and Xunli Zhang. Micromixing within microfluidic devices. *Topics in Current Chemistry*, 304(1):27–68, 2011.

[4] Zhuang Zhi Chong, Say Hwa Tan, Alfonso M Ganan-Calvo, Shu Beng Tor, Ngiap Hiang Loh, and Nam-Trung Nguyen. Active droplet generation in microfluidics. *Lab Chip*, 16:35–58, 2016.

[5] G F Christopher and S L Anna. Microfluidic methods for generating continuous droplet streams. *Journal of Physics D: Applied Physics*, 40(19):R319–R336, 2007.

[6] M. De Menech, P. Garstecki, F. Jousse, and H. a. Stone. Transition from squeezing to dripping in a microfluidic T-shaped junction. *Journal of Fluid Mechanics*, 595:141–161, 2008.

[7] Piotr Garstecki, Michael J. Fuerstman, Howard A. Stone, and George M. Whitesides. Formation of droplets and bubbles in a microfluidic T-junctionscaling and mechanism of break-up. *Lab on a Chip*, 6(3):437, 2006.

[8] Clement Kleinstreuer. *Microfluidics and Nanofluidics: Theory and Selected Applications: Theory and Selected Applications*. 2013.

[9] Princeton Microfluidics. Microfluidics Bootcamp 2014. 2014.

[10] Lingling Shui, J. C T Eijkel, and Albert van den Berg. Multiphase flow in micro- and nanochannels. *Sensors and Actuators, B: Chemical*, 121(1):263–276, 2007.

[11] Lingling Shui, Jan C T Eijkel, and Albert van den Berg. Multiphase flow in microfluidic systems - Control and applications of droplets and interfaces. *Advances in Colloid and Interface Science*, 133(1):35–49, 2007.

[12] Thomas Ward, Magalie Faivre, Manouk Abkarian, and Howard A. Stone. Microfluidic flow focusing: Drop size and scaling in pressure versus flow-rate-driven pumping. *Electrophoresis*, 26(19):3716–3724, 2005.

[13] Chun Guang Yang, Zhang Run Xu, and Jian Hua Wang. Manipulation of droplets in microfluidic systems. *TrAC - Trends in Analytical Chemistry*, 29(2):141–157, 2010.

[14] Chun Xia Zhao and Anton P J Middelberg. Two-phase microfluidic flows. *Chemical Engineering Science*, 66(7):1394–1411, 2011.